

# Kagome goldene with flat bands and Dirac nodal line fermions via line-graph epitaxy

Qiwei Tian<sup>1</sup>, Sahar Izadi Vishkayi<sup>2</sup>, Chen Zhang<sup>1</sup>, Jiang Zeng<sup>1</sup>, Bo Li<sup>1</sup>, Li Zhang<sup>1</sup>, Long-Jing Yin<sup>1</sup>, Yuan Tian<sup>1</sup>, Meysam Bagheri Tagani<sup>3\*</sup>, Lijie Zhang<sup>1\*</sup>, and Zhihui Qin<sup>1\*</sup>

1. *Key Laboratory for Micro/Nano Optoelectronic Devices of Ministry of Education & Hunan Provincial Key Laboratory of Low-Dimensional Structural Physics and Devices, School of Physics and Electronics, Hunan University, Changsha 410082, China*
2. *School of Physics, Institute for Research in Fundamental Sciences (IPM), P. O. Box 19395-5531, Tehran, Iran*
3. *Department of Physics, University of Guilan, P.O. Box 41335-1914, Rasht, Iran*

\*Corresponding authors:

lijiezhang@hnu.edu.cn; m\_bagheri@guilan.ac.ir; zhqin@hnu.edu.cn;

## **Abstract**

The kagome lattice is a promising platform for exploring exotic quantum phases. However, achieving a single-atomic-layer kagome lattice in elemental materials has remained a significant challenge. Here we introduce line-graph epitaxy, a novel approach that enables the synthesis of single-atomic-layer goldene with a kagome lattice. Through scanning tunneling microscopy (STM) and spectroscopy (STS), alongside density functional theory (DFT) calculations, we provide direct evidence of kagome goldene, which exhibits a flat band with a van Hove singularity  $\sim 1.1$  eV below the Fermi level—indicative of strong electron correlation effects. Notably, the flat band breaks down at the zigzag edges of the goldene nanoflakes, underlining the role of edge effects. Additionally, our calculations reveal that weak interlayer interactions between goldene and the Au<sub>2</sub>Ge substrate give rise to dual Dirac nodal lines due to a proximity effect. These findings offer a strategy for constructing elemental kagome lattices and provide a generalizable approach for fabricating and controlling line-graph materials. This work paves the way for exploring quantum phases driven by strong correlations and designing materials for quantum technologies.

The crystal structure with a kagome lattice has been regarded as an ideal motif for geometric frustration in quantum spin liquids<sup>1-6</sup>. Based on the fundamental concepts in graph theory, the kagome lattice is the line graph of a honeycomb structure, where each vertex represents an edge of the original graph, and a new graph is constructed by connecting vertices that share an edge in the original structure. It was first introduced by placing an additional spin at the midpoint of each bond in a honeycomb lattice to obtain the exact solution for an antiferromagnet<sup>7</sup>. Many bulk systems are found to contain kagome lattices, exhibiting a range of phenomena, including magnetic properties, superconductivity, electron nematic phases, pair charge density waves, and so on<sup>8-15</sup>. However, the individual kagome layers are interspersed with non-kagome atoms/layers, making it challenging to explicitly probe their intrinsic properties.

Monoatomic layers of metals, in contrast to other two-dimensional (2D) materials with covalent bonding, are composed of metallic bonding, which can expand the range of 2D materials and their potential applications. An experimental breakthrough in the realization of a single-atom layer of iron has inspired the pursuit of 2D metals<sup>16</sup>. Gold (Au) is known as the most stable metal, and its low-dimensional forms have garnered significant attention due to their wide range of feasible applications<sup>17-20</sup>. Recently, a single-atom layer of Au, goldene, was synthesized using a wet chemical method<sup>21,22</sup> and on-surface synthesize methods<sup>23,24</sup>. Since kagome lattice configurations are often associated with strongly correlated phenomena and nontrivial band topology<sup>25-31</sup>, there is a strong desire to realize a metallic single-atom layer with a kagome lattice<sup>32,33</sup>, which is believed to hold great potential of designing quantum phases. However, achieving this in a solid-state system remains a significant challenge<sup>34-39</sup>.

In this work, we introduce the line-graph epitaxy of gold atoms on Au<sub>2</sub>Ge with honeycomb lattice, where the growth of gold occurs along the edges of the line-graph derived from the substrate, enabling the realization of kagome goldene with flat bands and proximity effect induced Dirac nodal line (DNL) fermions. By combining scanning tunneling microscopy/spectroscopy (STM/STS) with density functional theory (DFT) calculations, we investigate the structural and electronic properties of the constructed kagome goldene system on topological DNL Au<sub>2</sub>Ge. Theoretical calculations reveal that the weak interlayer interaction between Au<sub>2</sub>Ge and kagome goldene promotes the emergence of dual DNL due to the proximity. A flat band exhibiting the characteristic van Hove singularity appears at  $\sim 1.1$  eV below the Fermi level, as confirmed by both STS measurements and DFT calculations. Moreover, this flat band is disrupted at the zigzag edge of the kagome goldene, and electronic states emerge at positive energies near the Fermi level due to quantum confinement and edge arrangement modifications of the goldene nanoislands.

We selected Au<sub>2</sub>Ge, previously synthesized<sup>40</sup>, which consists of a honeycomb Au lattice and a triangular Ge lattice<sup>40</sup>, as a template. Au atoms occupy the midpoints of the polyline derived from the underlying substrate, forming a single atomic layer of goldene with a kagome lattice structure. Figure 1a illustrates a schematic of how the kagome lattice is constructed from the triangular lattice surface, where gray (black) dots labeled A (B) represent Ge (Au) atoms in Au<sub>2</sub>Ge, respectively. The red dots labeled C represent the topmost Au atoms that form the kagome layer. It is crucial to determine the epitaxial relationship between the topmost kagome layer and the underlying Au<sub>2</sub>Ge substrate. An STM topographic image of Au<sub>2</sub>Ge is shown in Fig. 1b, along with its ball-and-stick model

(see inset). Au atoms segregate to the Au<sub>2</sub>Ge surface upon annealing at high temperature for approximately 1 hour, forming a kagome lattice. As a result, the stacking sequence of the kagome goldene, Au<sub>2</sub>Ge, and the Au(111) substrate is depicted in the model shown in Fig. 1c. Figure 1d presents an STM topographic image of the resulting layer, which appears as an island with a kagome lattice structure. The apparent height difference between the kagome layer and the underlying layer is approximately 230 pm, indicating the presence of a single-atom-layer feature (see Fig. 1e). In order to exclude the possibility of Ge terminating, we performed DFT calculations by placing three Ge atoms with an initial kagome lattice configuration on top of the Au<sub>2</sub>Ge substrate. However, the structure transforms to a triangular lattice, with the bond length between Ge atoms measuring approximately 2.78 Å. Additionally, Ge<sub>3</sub> is no longer coplanar, with one Ge atom positioned about 0.4 Å lower than the other two. Moreover, the Au<sub>2</sub>Ge substrate is also not flat (see Supplementary Fig. 1). Therefore, we can rule out the possibility of a Ge kagome structure. Instead, we propose a model in which an atomic layer of kagome Au is located on top of the Au<sub>2</sub>Ge substrate. Figure 1f shows a typical STM topographic image of the obtained structure, while Figure 1g provides an enlarged view clearly displaying the kagome lattice. These periodicities are further confirmed in the fast Fourier transform (FFT) of the STM topography (Fig. 1h) and by the line profiles shown in Fig. 1i. The distance between the nearest Au atoms in the kagome lattice is measured to be ~2.48 Å, which is about  $\sqrt{3}/2$  times the lattice constant of Au(111), approximately 2.49 Å.

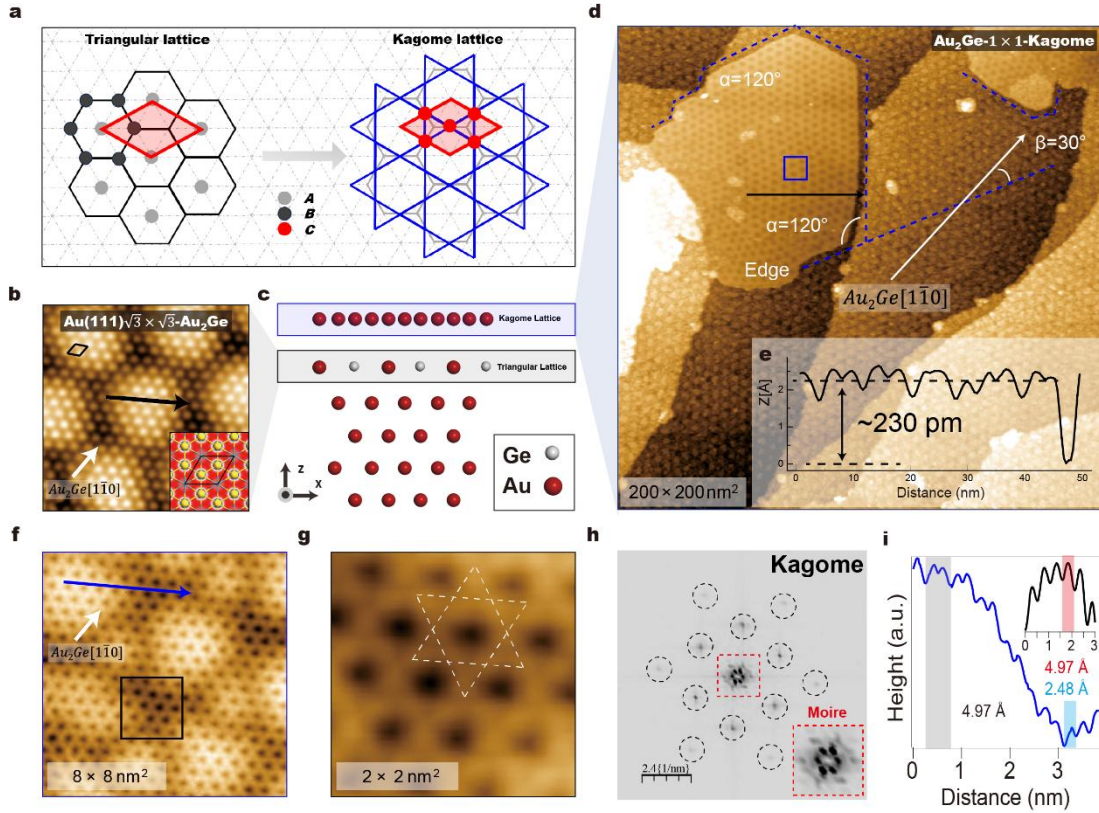


**Fig. 1 | Synthesis process of kagome goldene.** **a**, Design principle from honeycomb lattice to kagome lattice. **b**, Atomic resolution STM topographic image of  $\text{Au}_2\text{Ge}$  with its model inset. **c**, Side view of structure model for the stacking of kagome goldene,  $\text{Au}_2\text{Ge}$  and  $\text{Au}(111)$ . **d**, Large-scale STM topographic image of  $\text{Au}_2\text{Ge}-1 \times 1$ -kagome. **e**, The apparent height difference between kagome layer and under layer is about 230 pm. **f**, High resolution STM topographic images of kagome layer. **g**, Zoom-in atomic resolution, STM image of kagome layer. **h**, Fast Fourier transform image obtained from STM image of (f). The black dash circles show reciprocal lattice of kagome structure, whereas the inset show the reciprocal moiré lattice. **i**, Line profiles for  $\text{Au}_2\text{Ge}$  and kagome layer follow the corresponded blue and black lines shown in (b) and (f), respectively. Scanning conditions are as follows: (b)  $V_S = -10$  mV,  $I_T = 1000$  pA; (d)  $V_S = -100$  mV,  $I_T = 1000$  pA; (f-g)  $V_S = -100$  mV,  $I_T = 1000$  pA.

To form the kagome network of gold on  $\text{Au}_2\text{Ge}$ , it is essential for the gold atoms to occupy the Au-Au bridge sites of the  $\text{Au}_2\text{Ge}$  substrate. Initially, we investigate the reasons for the positioning of gold atoms in a kagome structure on the Au-Au bridge of the substrate. Figure 2a shows the energy difference between the most stable stacking of kagome/ $\text{Au}_2\text{Ge}$

and various stackings. The most stable configuration is placing kagome lattice on the bridge sites of Au-Au of the substrate. The stackings are obtained by shifting the kagome sheet on the Au<sub>2</sub>Ge substrate with different combinations of the lattice vectors  $\mathbf{a}_1$  and  $\mathbf{a}_2$  where zero energy indicating the stable configuration of the system. In this study,  $(\mathbf{a}_1, \mathbf{a}_2) = (0, 0), (1, 0), (0, 1), (1, 1)$  means the kagome structure is positioned on the Au-Au bridge. As shown, the most stable configuration is the kagome structure on the Au-Au bridge. The energy difference between this configuration and others can reach up to 700 meV. In the most stable arrangement, the vertical distance between the two layers is 2.8 Å. The two configurations with the lowest and highest energies are shown in Fig. 2b. In the stable arrangement, the distance between the gold atoms of the two layers is 3.16 Å, while in the least stable configuration, this distance is 2.91 Å. In the most stable arrangement, the Ge atoms of the substrate are exactly at the center of the hexagons of the kagome structure, and the gold atoms are at the center of the triangles. Changing this symmetry results in a decrease in stability energy, such that a symmetric charge density pattern is not observed for the unstable structure. The relationship between the change in structure configuration and the electronic properties of the gold kagome lattice is examined in Fig. 2d-e. In the less stable structure, a very strong hybridization between Au<sub>2</sub>Ge and kagome occurs, eliminating all the features of a kagome structure, including the flat band, van Hove singularity, and Dirac point. In contrast, for the kagome lattice located on the Au-Au bridge of the Au<sub>2</sub>Ge monolayer, the features of the kagome lattice are well observed in the density of states. To investigate the behavior of a gold atom placed at the Au-Au bridge position over time, we performed ab-initio molecular dynamics (AIMD) simulations in the NVT

ensemble at 500K for 4 ps. As shown in the Supplementary Fig. 2, the gold atom moves on the Au<sub>2</sub>Ge structure and never deviates from it during the 4ps duration.

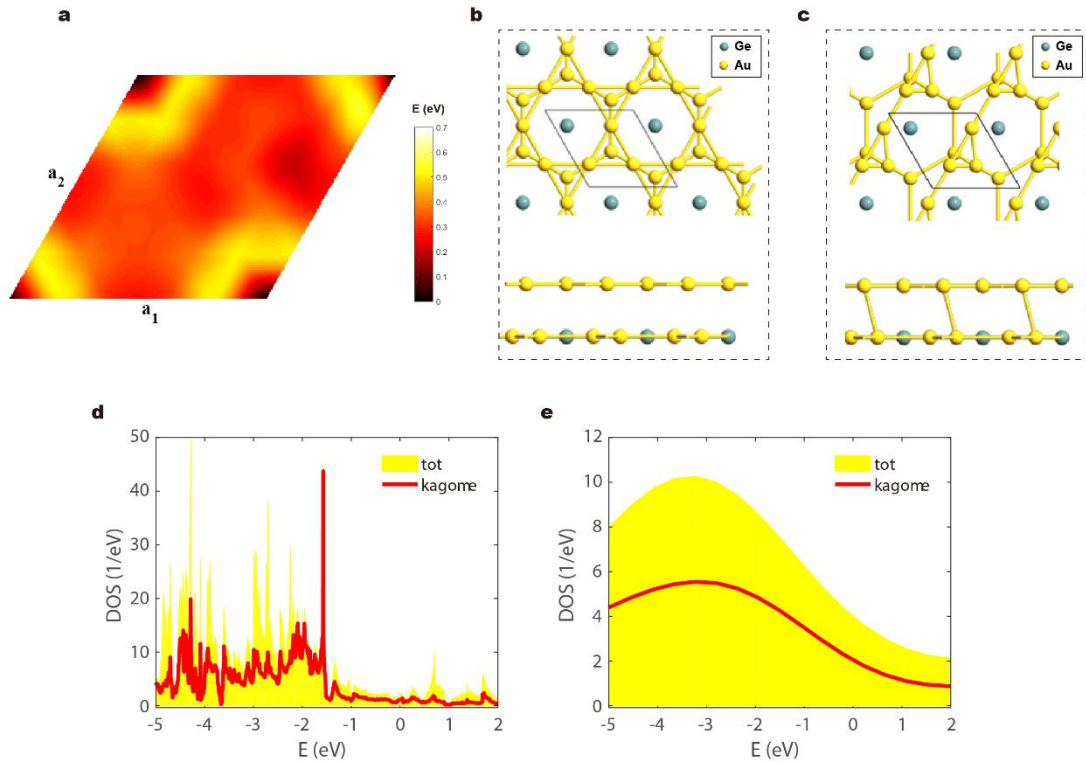


**Fig. 2 | Formation mechanism and stabilization of kagome goldene.** **a**, The figure shows the energy difference between the most stable stacking of kagome/Au<sub>2</sub>Ge and various stackings. The most stable configuration is placing kagome lattice on the bridge sites of Au-Au of the substrate. The stackings are obtained by shifting the kagome sheet on the Au<sub>2</sub>Ge substrate with different combinations of the lattice vectors **a**<sub>1</sub> and **a**<sub>2</sub>. **b** and **c**, Top and side views of the most stable and less stable stacking of the kagome goldene on top of monolayer Au<sub>2</sub>Ge. **d** and **e**, Total and projected density of states for the most stable and unstable configurations, respectively.

To gain deeper insights into the obtained structure, we conducted DFT calculations to examine the electronic properties of both free-standing and substrate-supported kagome goldene. Based on the model described above, we examine a single atomic layer of Au forming a kagome lattice on a monolayer of Au<sub>2</sub>Ge, where each Ge atom in the bottom layer is positioned at the center of the hexagons. The optimized bond length in the Au<sub>2</sub>Ge

layer is 2.78 Å, whereas the bond length is 2.40 Å in the kagome lattice, which are in agreement with the experiments as indicated in the line profiles in Fig. 1i. The Au<sub>2</sub>Ge layers are nearly flat, with a corrugation of approximately 5 pm, while the kagome lattice remains completely flat. Figure 3a presents, side by side, the relaxed atomic structure model, the simulated STM image, and the experimental atomic-resolved STM image of the kagome goldene. The simulated STM results are in excellent agreement with the experimental observations, confirming the consistency between the experimental and theoretical models.

We now investigate the electronic properties of the considered structure. When spin-orbit coupling (SOC) is considered, as depicted in Fig. 3b, a nearly flat band is maintained along the M-K path, and type-I and type-II Dirac points are observed. Without SOC, as shown in Supplementary Fig. 3, the band structure reveals nearly flat bands, with Dirac points present at both positive and negative energy levels. Additionally, van Hove singularities appear at negative energy levels. It is important to note that the flat bands and van Hove singularities occur at close energy levels, contributing to sharp peaks in the density of states (DOS) for each scenario. The presence of the Dirac cone and the flat band are the inherent characteristics of kagome structure. The band structure of the kagome goldene differs from that of the ideal kagome lattice in two aspects. First, the band is not completely flat, but has a finite bandwidth in a part of the first Brillouin zone. Second, there is a gap between the band and the two bands forming the Dirac cone. These features can be attributed to the effects of the d-orbitals of Au atoms, the periodic potential from the Au<sub>2</sub>Ge layer, and the second-neighbor hopping in the kagome lattice.

We then perform STS measurements on the kagome goldene to experimentally probe its electronic properties. Figure 3c shows the differential conductance ( $dI/dV$ - $V$  spectra) of

the surface, which is proportional to the local density of states (LDOS). The measurements, conducted along the line marked in the inset of Fig. 3c, reveal the uniform electronic features of the kagome layer. In Fig. 3d, we present the  $dI/dV$  spectrum taken from an arbitrary position on the kagome goldene, marked by a black cross in the inset of Fig. 3c. The spectra exhibit three dominant peaks, located at approximately -0.26 V, -0.6 V, and -1.1 V, labeled as  $\alpha$ ,  $\beta$ , and  $\gamma$ , respectively. The sharp peak in the  $dI/dV$  spectrum, corresponding to the large DOS of the electronic flat bands, is clearly visible in the STS measurements<sup>41</sup>. We then carry out first-principles calculations to compare the theoretical DOS with the experimental observations. Figure 3d also shows the calculated DOS alongside the experimental data, based on the band structure presented in Fig. 3b. At negative energies, three main peaks are observed. The first two peaks, located around -0.5 eV and -0.8 eV, are primarily attributed to the tilted Dirac points. The third peak, located at approximately -1.4 eV, is due to the nearly flat band and van Hove singularity, which is consistent with the band structure shown in Fig. 3b. By combining the STS measurements with DFT calculations, we find that the synthesized kagome goldene simultaneously exhibits three features of a flat band, van Hove singularities, and a Dirac cone, the typical characteristics of kagome lattice. Further  $dI/dV$  mappings at different energies (-0.3 V, -0.6 V, and -1.1 V) reveal that the electrons are confined to the center of the kagome structure (Fig. 3e). This behavior is attributed to the geometric frustration of the lattice<sup>42</sup>.

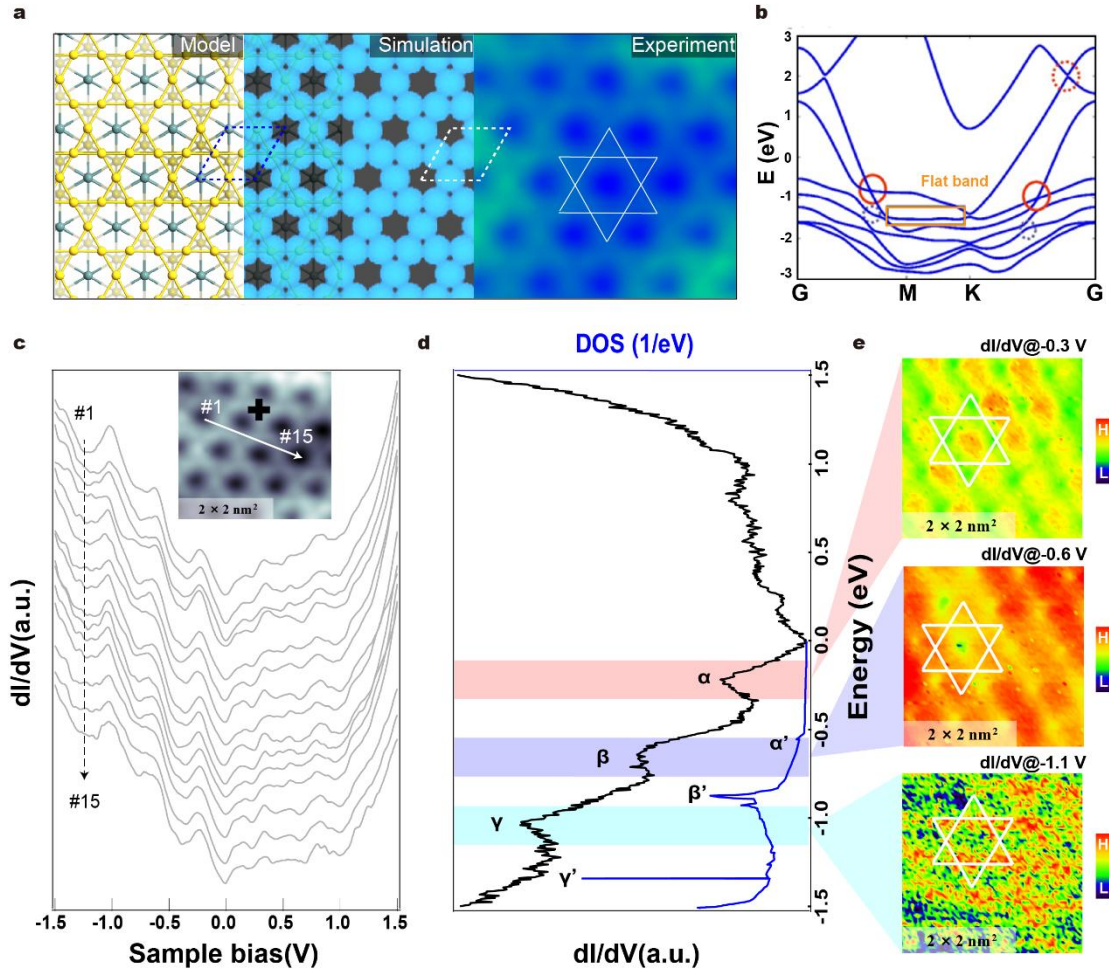


**Fig. 3 | Calculated band structure and tunneling spectroscopy of goldene. a**, Left: Ball-and-stick model. Yellow dots represent Au atoms. Middle: Simulated STM image of kagome goldene. Right: Experimental STM image of kagome goldene (set points:  $V_s = -100$  mV,  $I_T = 1000$  pA). **b**, Band structure of kagome goldene with considering spin-orbit coupling. The rectangular shows the nearly flat band, and dashed (solid) large circles indicate type-I (type-II) Dirac points. Small dashed circles show the van Hove singularity points. **c**, Differential conductance spectra on the surface, taken along the direction marked with a white line in the inset STM topographic image. Inset: a typical STM image of kagome lattice (set points:  $V_s = -100$  mV,  $I_T = 1000$  pA). **d**, Typical  $dI/dV$  spectra recorded on kagome lattice and DOS of the kagome goldene. **e**,  $dI/dV$  maps at various voltages of  $-0.3$  V,  $-0.6$  V and  $-1.1$  V, respectively.

Our experimental investigations have confirmed the presence of nanoislands with a kagome structure (Fig. 4a and its inset). The edge information at atomic level can be extracted from the inset image. A special type of zigzag edge is found as shown in Fig. 4b. STS measurements clearly show the disappearance of the peak in the  $dI/dV$  spectrum at

occupied states (see Fig. 4c), revealing the breakdown of flat band at the zigzag edges. Whereas, edge states are detected at positive energies (Fig. 4c). The electronic states detected on these nanoislands diverge markedly from those on the extended kagome sheets. To elaborate the underlying physics and the influence of edge states on the electronic characteristics, we conducted simulations of the nanoisland configurations. We compared the DOS from each gold atom on nanoislands with that from an ideal kagome lattice atom, as illustrated in Fig. 4d. It is evident that quantum confinement and edge arrangement modifications of the nanoislands exert a profound impact on the electronic properties relative to a complete sheet. Our findings align closely with experimental observations, particularly for nanoislands with zigzag edges. In these cases, the pronounced peak associated with the flat band is mitigated, and electronic states at positive energies emerge near the Fermi level. The predominant contributions arise from the atomic configurations at the zigzag edges and the wave functions at positive energies diminish exponentially as they penetrate the island's interior (refer to Fig. 4e). Furthermore, the localized states within the kagome lattice's triangular motifs are instrumental in the manifestation of this peak (see Fig. 4e). These findings elucidate the tunability of the kagome lattice's electronic properties through strategic manipulation of the edge topologies of nanoislands.

Examination of the STS results shows that, unlike the kagome sheet, the edges exhibit electronic states at an energy of approximately 0.5 eV, while the peaks corresponding to -1.0 eV are suppressed. To further investigate this behavior, we analyze the edge of the semi-infinite kagome structure using surface Green's functions and Wannier functions, employing the WannierTools computational code<sup>43</sup>. This approach allows us to explore the electronic properties at the edges in greater detail, providing insights into the distinct edge

states and their contribution to the overall electronic structure of the kagome system. Comparing the bulk and ribbon-edge band structures as shown in Fig. 4f, the interior kagome structure exhibits numerous electronic states around -0.8 eV. In contrast, at the ribbon edge, we observe the emergence of electronic states at 0.4 eV, while the states at -0.8 eV are suppressed. These findings, aligning with experimental observations, demonstrate that the edge of the kagome structure exhibits distinct electronic states compared to the interior. Additionally, the Dirac cones associated with the bulk structure are absent at the edge, further emphasizing the unique electronic properties of the kagome edges.

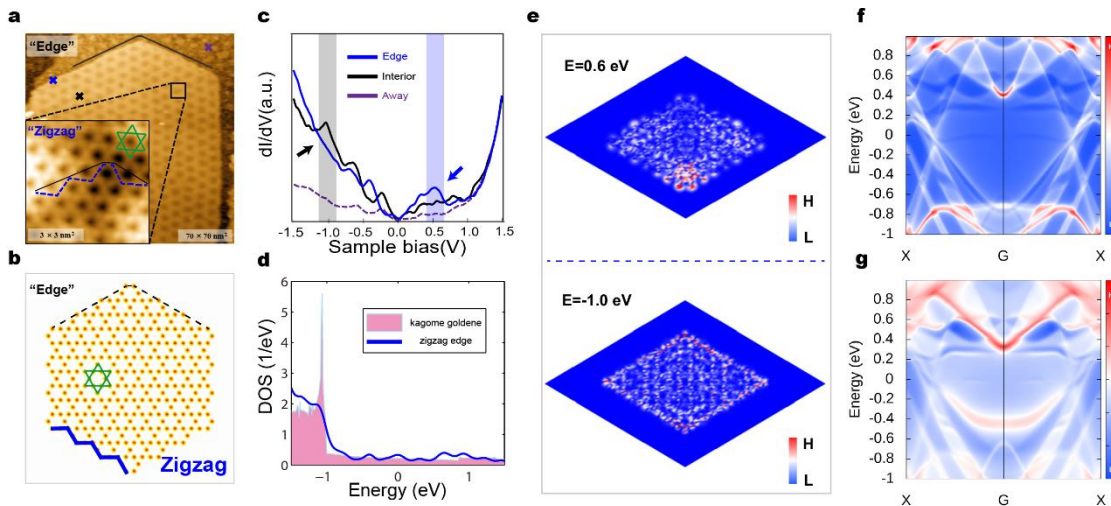


**Fig. 4 | Edge information in goldene.** **a**, STM image of kagome goldene with zigzag edge. Inset: atomic resolution STM image of kagome goldene. **b**, Top views of the atomic structure of the kagome goldene with zigzag edge. **c**, Differential conductance spectra of edge, interior, and away the island marked by various colored crosses in (a). **d**, DOS of the perfect kagome goldene sheet and kagome nanoislands with zigzag edge arrangements, respectively. **e**, Wave function of kagome nanoisland at energy of  $E=0.6$  eV (Top panel) and  $E=-1$  eV (Bottom panel), respectively. **f-g**, Band structures of bulk (f) and ribbon edge (g), respectively. Scanning conditions are as follows: (a)  $V_s = -100$  mV,  $I_T = 1000$  pA.

We then consider the heterostructure formed by kagome goldene and  $Au_2Ge$ . On a larger scale, it is worth noting that there is a much larger periodicity corresponding to the

inner dots in the FFT image shown in Fig. 1f, indicating the presence of a moiré pattern, which is visible in the large-scale STM topographic image, as shown in the inset of Fig. 5a. We mark the different stacking sites of the moiré pattern as TOP, HCP, and FCC, respectively. The pattern consists of alternating bright and dark spots, forming a distinct moiré structure by overlaying Au<sub>2</sub>Ge on the Au(111) substrate. Since the kagome goldene layer is located on top of the Au<sub>2</sub>Ge surface, the periodicity of the moiré pattern is approximately 4.05 nm (inset Fig. 5a). The formation mechanism of the moiré pattern is illustrated in Fig. 5b, where side- and top-view images of the stacking of goldene on Au<sub>2</sub>Ge, supported by the Au(111) substrate, are clearly shown. The calculated band structure of the entire system is shown in Fig. 5c. As can be seen, there are three bands crossing the Fermi level, with four Dirac points observed along the M- $\Gamma$  and K- $\Gamma$  directions around the Fermi level. Additionally, a Dirac cone is observed along the M- $\Gamma$  and K-- $\Gamma$  direction at an energy of approximately -0.4 eV. Some nearly flat bands also appear around -1.7 eV, below the Dirac cone. The Fermi surface of the structure is shown in Fig. 5d, where two distinct DNLs are clearly visible, with their vortices locating along the M- $\Gamma$  direction, consistent with the band structure. In our previous work, we have reported that the Au<sub>2</sub>Ge monolayer also exhibits a DNL in its electronic band structure<sup>40</sup>. Here, we investigate the effect of stacking of kagome goldene on Au<sub>2</sub>Ge, finding that this bilayer structure, not only preserves the DNL of the Au<sub>2</sub>Ge monolayer, but also generates another DNL in the Au layer, whose nodes are located at the K and M points of the Brillouin zone. We attribute this phenomenon to the weak interlayer interaction that maintains the DNL of each layer and allows the emergence of two DNLs in kagome goldene layer due to the proximity effect. The preservation and doubling of DNLs are significant features, which have important

applications in spintronics, valleytronics, and topological devices. The layer projected band structure is depicted in Fig. 5e-f, top and bottom panel for kagome layer, and Au<sub>2</sub>Ge, respectively. As it is clear, two Dirac points belong to the monolayer kagome goldene layer. Also, the almost flat bands observed in the band structure around -1.7 eV belong to the kagome lattice. The comparison of density of states of goldene/Au<sub>2</sub>Ge heterostructure with isolated kagome goldene on Au<sub>2</sub>Ge shows that the interlayer interaction is very weak, leading to the preserving DNLs. The DNLs in the kagome goldene are also protected by the mirror reflection symmetry, which arises from the planar geometry of each layer. The observed behavior is accord with the experimental STS results. A shift in the location of the peaks compare to the experimental results is due to electron injection from the substrate to the goldene/Au<sub>2</sub>Ge heterostructure<sup>44</sup>. The Bader charge analysis reveals that amount of  $6 \times 10^{13} \text{ cm}^{-2}$  electron is transferred from the substrate to goldene/Au<sub>2</sub>Ge heterostructure. We perform differential conductance spectroscopy (see Fig. 5g) at typical positions on the moiré pattern, as highlight in the inset of Fig. 5g, and find that the results are similar to those of the atomic structure of the single kagome layer aforementioned. It is well known that  $dI/dV$  maps reveal spatial variations in the differential conductance across the sample at given energies. We perform  $dI/dV$  mapping at three selected energies, where the differential conductance exhibits distinct specific-stackings related intensity variations (see Fig. 5h).

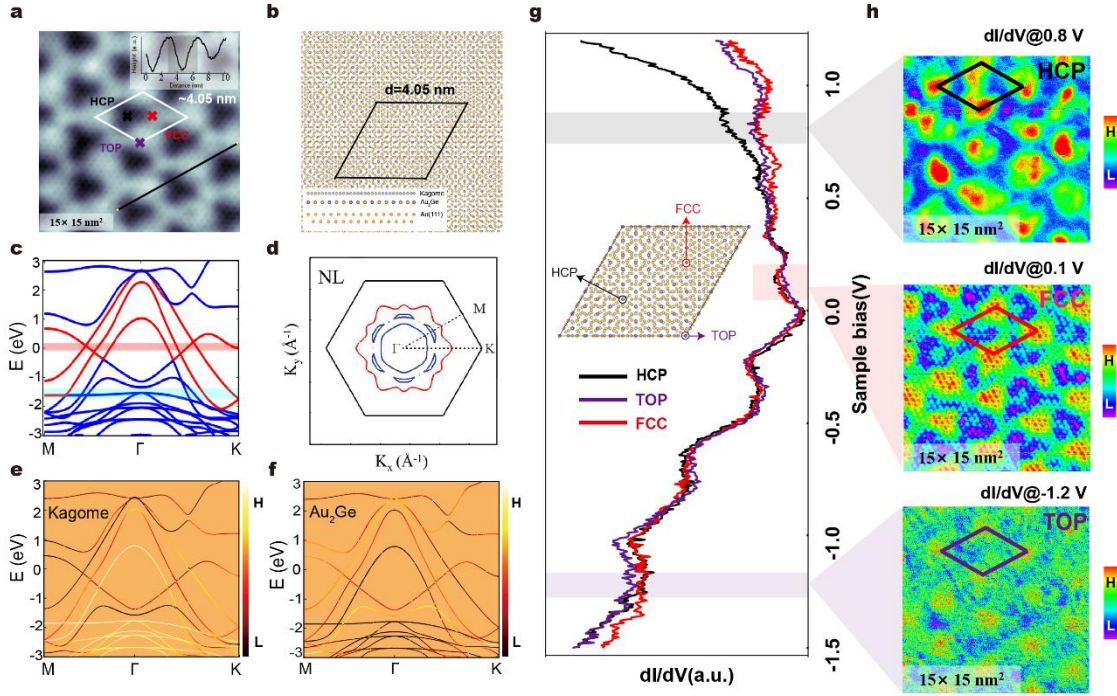


**Fig. 5 | Structural and electronic properties of heterostructure of goldene/Au<sub>2</sub>Ge.** **a**, Typical STM image of moiré pattern by kagome goldene on Au<sub>2</sub>Ge supported by Au(111). Inset: line profile follow the line marked in **a**. **b**, Large-scale ball and stick model for the stacked kagome goldene/Au<sub>2</sub>Ge/Au(111). Inset: side view of the atom model for kagome/Au<sub>2</sub>Ge/Au(111). **c**, Band structure of goldene/Au<sub>2</sub>Ge heterostructure. **d**, The Fermi surface of the goldene layer. **e-f**, Projected band structure of kagome goldene (**e**) and monolayer Au<sub>2</sub>Ge (**f**), respectively. **g**, Typical  $dI/dV$  spectra recorded at three different positions as marked in inset STM image of kagome goldene with a moiré pattern (set points:  $V_S = -40$  mV,  $I_T = 500$  pA). Inset: schematic of different stacking regions with HCP, TOP and FCC, respectively. **h**,  $dI/dV$  maps at various voltages of -1.2 V, 0.1 V and 0.8 V, respectively.

In summary, our study demonstrates the realization and characterization of a single atomic layer of goldene with a kagome lattice on an Au<sub>2</sub>Ge substrate via line-graph epitaxy. The weak interlayer interaction between the kagome goldene layer and the Au<sub>2</sub>Ge substrate preserves the DNL of the underlying Au<sub>2</sub>Ge and the Dirac point of the kagome lattice, resulting in the coexistence of multiple DNLs due to the proximity effect. This unique bilayer structure exhibits significant electronic properties, including Dirac points and

nearly flat bands, characteristic of the kagome lattice. These features are confirmed through both experimental measurements and theoretical calculations. The electronic properties of the kagome lattice can be further tuned through the strategic manipulation of the nanoisland edges. The presence of Dirac cones, flat bands, and van Hove singularities in the synthesized single-layer Au structure underscores its potential applications in advanced electronic and spintronic devices. Our findings provide valuable insights into the electronic behavior of kagome lattices and open avenues for designing materials with tailored electronic properties for technological applications. We anticipate that our work will serve as a foundation for constructing line-graph lattice materials, extending beyond the kagome structure, and offering a robust strategy for precisely controlling lattice configurations.

## **Methods**

**Experimental details.** Our experiments were carried out in a CreaTec LT-STM system equipped with a home-built molecular beam epitaxy (UHV-MBE) chamber. The base pressure of the system is better than  $1 \times 10^{-10}$  Torr. The Au(111) substrate was cleaned by several circles of sputtering and annealing. Subsequently, molecular beam Ge (99.999%, Alfa Aesar) were thermally evaporated from a K-cell evaporator onto Au(111) substrate held at  $\sim 380^\circ\text{C}$ . All the STM/STS measurements were conducted at 77 K. The STS ( $dI/dV$ - $V$  curve) measurements were acquired by using a standard lock-in technique (793 Hz, 40-20 mV a.c. bias modulation). The system were carefully calibrate by the Au(111) surface.

**Calculation methods.** The Vienna *Ab-initio* Simulation Package<sup>45</sup> was used to calculate the electronic properties of the heterostructure using density functional theory. The generalized gradient approximation (GGA) was employed with the Perdew-Burke Ernzerhof (PBE) exchange-correlation functional<sup>46</sup>. The plane wave cutoff energy was 450

eV, and the energy self-consistent criteria was  $10^{-6}$  eV. To optimize the structures, the atomic positions and lattice sizes are fully relaxed using the conjugate gradient algorithm until the Hellman-Feynman forces drop below  $10^{-2}$  eV/Å. The kagome goldene layer was build according to the experimental findings. The Brillouin zone was sampled by a  $20 \times 20 \times 1$  Monkhorst-Pack k-point grid, and the DFT-D3 dispersion correction by Grimme is adopted to account for the van der Waals interactions<sup>47</sup>. A vacuum of 20 Å was considered to avoid the interaction between the systems with its image. The Au slab is composed of three gold layers where two bottom layers were fixed during the optimization.

### **Data availability**

The authors declare that the data supporting the findings of this study are available within the paper and its Supplementary Information files. The data that support the findings of this study are also available from the corresponding authors upon request.

**Author Contributions:** Q.T. performed the STM experiments and analyzed the data. S.I.V. and M.B.T. performed the theoretical calculations. Lijie Zhang and Z.Q. supervised the project. Q.T., M.B.T., Lijie Zhang and Z.Q. wrote the manuscript with inputs from all the other authors. All authors discussed the data and contributed to the final editing of the paper.

### **Acknowledgements**

This work was supported by the National Key R&D Program of China (2024YFF0727104), the National Natural Science Foundation of China (Grant Nos. 12174096, 51972106, 12174095 and 12204164), the Strategic Priority Research Program of Chinese Academy of Sciences (Grant No. XDB30000000), the Natural Science Foundation of Hunan Province, China (Grant No. 2021JJ20026), and the Science and Technology Innovation Program of Hunan Province, China (Grant No. 2021RC3037).

## References:

- 1 Zhou, Y., Kanoda, K. & Ng, T. K. Quantum spin liquid states. *Rev. Mod. Phys.* **89**, 025003 (2017).
- 2 Yan, S. M., Huse, D. A. & White, S. R. Spin-Liquid Ground State of the  $S=1/2$  Kagome Heisenberg Antiferromagnet. *Science* **332**, 1173-1176 (2011).
- 3 Balents, L. Spin liquids in frustrated magnets. *Nature* **464**, 199-208 (2010).
- 4 Norman, M. R. Colloquium: Herbertsmithite and the search for the quantum spin liquid. *Rev. Mod. Phys.* **88**, 041002 (2016).
- 5 Shores, M. P., Nytko, E. A., Bartlett, B. M. & Nocera, D. G. A structurally perfect  $S = 1/2$  kagome antiferromagnet. *J. Am. Chem. Soc.* **127**, 13462-13463 (2005).
- 6 Helton, J. S. *et al.* Spin dynamics of the spin-1/2 Kagome lattice antiferromagnet  $\text{ZnCu}_3(\text{OH})_6\text{Cl}_2$ . *Phys. Rev. Lett.* **98**, 107204 (2007).
- 7 Syôzi, I. Statistics of Kagomé Lattice. *Prog. Theor. Phys.* **6**, 306-308 (1951).
- 8 Ye, L. *et al.* Massive Dirac fermions in a ferromagnetic kagome metal. *Nature* **555**, 638-642 (2018).
- 9 Yin, J.-X. *et al.* Giant and anisotropic many-body spin-orbit tunability in a strongly correlated kagome magnet. *Nature* **562**, 91-95 (2018).
- 10 Zhao, H. *et al.* Cascade of correlated electron states in the kagome superconductor  $\text{CsV}_3\text{Sb}_5$ . *Nature* **599**, 216-221 (2021).
- 11 Liu, D. F. *et al.* Magnetic Weyl semimetal phase in a Kagome crystal. *Science* **365**, 1282-1285 (2019).
- 12 Chen, H. *et al.* Roton pair density wave in a strong-coupling kagome superconductor. *Nature* **599**, 222-228 (2021).
- 13 Mielke, C. *et al.* Time-reversal symmetry-breaking charge order in a kagome superconductor. *Nature* **602**, 245-250 (2022).
- 14 Nie, L. *et al.* Charge-density-wave-driven electronic nematicity in a kagome superconductor. *Nature* **604**, 59-64 (2022).
- 15 Sun, Z. *et al.* Observation of Topological Flat Bands in the Kagome Semiconductor  $\text{Nb}_3\text{Cl}_8$ . *Nano Lett.* **22**, 4596-4602 (2022).
- 16 Zhao, J. *et al.* Free-Standing Single-Atom-Thick Iron Membranes Suspended in Graphene Pores. *Science* **343**, 1228-1232 (2014).
- 17 Ohnishi, H., Kondo, Y. & Takayanagi, K. Quantized conductance through individual rows of suspended gold atoms. *Nature* **395**, 780-783 (1998).
- 18 Yanson, A., Bollinger, G. R., Van den Brom, H., Agrait, N. & Van Ruitenbeek, J. Formation and manipulation of a metallic wire of single gold atoms. *Nature* **395**, 783-785 (1998).
- 19 Häkkinen, H., Moseler, M. & Landman, U. Bonding in Cu, Ag, and Au clusters: Relativistic Effects, Trends, and Surprises. *Phys. Rev. Lett.* **89**, 033401 (2002).
- 20 Oshima, Y., Onga, A. & Takayanagi, K. Helical gold nanotube synthesized at 150 K. *Phys. Rev. Lett.* **91**, 205503 (2003).
- 21 Kashiwaya, S. *et al.* Synthesis of goldene comprising single-atom layer gold. *Nat. Synth.* **3**, 744-751 (2024).
- 22 Peplow, M. Meet 'goldene': this gilded cousin of graphene is also one atom thick. *Nature* **629**, 17-17 (2024).
- 23 Preobrajenski, A. *et al.* Boron-induced transformation of ultrathin Au films into two-dimensional metallic nanostructures. *Nat. Commun.* **15**, 10518 (2024).
- 24 Forti, S. *et al.* Semiconductor to metal transition in two-dimensional gold and its van der Waals heterostack with graphene. *Nat. Commun.* **11**, 2236 (2020).

- 25 Yin, J.-X., Lian, B. & Hasan, M. Z. Topological kagome magnets and superconductors. *Nature* **612**, 647-657 (2022).
- 26 Kang, M. *et al.* Topological flat bands in frustrated kagome lattice CoSn. *Nat. Commun.* **11** (2020).
- 27 Mendels, P. *et al.* Quantum magnetism in the paratacamite family: Towards an ideal kagome lattice. *Phys. Rev. Lett.* **98** (2007).
- 28 Tang, E., Mei, J.-W. & Wen, X.-G. High-Temperature Fractional Quantum Hall States. *Phys. Rev. Lett.* **106** (2011).
- 29 Yu, S.-L. & Li, J.-X. Chiral superconducting phase and chiral spin-density-wave phase in a Hubbard model on the kagome lattice. *Phys. Rev. B* **85** (2012).
- 30 Kiesel, M. L., Platt, C. & Thomale, R. Unconventional Fermi Surface Instabilities in the Kagome Hubbard Model. *Phys. Rev. Lett.* **110** (2013).
- 31 Neupert, T., Denner, M. M., Yin, J.-X., Thomale, R. & Hasan, M. Z. Charge order and superconductivity in kagome materials. *Nat. Phys.* **18**, 137-143 (2022).
- 32 Kim, S. W., Oh, H., Moon, E. G. & Kim, Y. Monolayer Kagome Metals  $AV_3Sb_5$ . *Nat. Commun.* **14**, 591 (2023).
- 33 Zhou, H., dos Santos Dias, M., Zhang, Y., Zhao, W. & Lounis, S. Kagomerization of transition metal monolayers induced by two-dimensional hexagonal boron nitride. *Nat. Commun.* **15**, 4854 (2024).
- 34 Peng, S. *et al.* Realizing Kagome Band Structure in Two-Dimensional Kagome Surface States of  $RV_6Sn_6$  ( $R = Gd, Ho$ ). *Phys. Rev. Lett.* **127**, 266401 (2021).
- 35 Lin, Y.-H. *et al.* Fabrication and Imaging Monatomic Ni Kagome Lattice on Superconducting Pb(111). *Nano Lett.*, 8475-8481 (2022).
- 36 Sun, S. *et al.* Designing Kagome Lattice from Potassium Atoms on Phosphorus-Gold Surface Alloy. *Nano Lett.* **20**, 5583-5589 (2020).
- 37 Baddeley, C. J., Stephenson, A. W., Hardacre, C., Tikhov, M. & Lambert, R. M. Structural and electronic properties of Ce overlayers and low-dimensional Pt-Ce alloys on Pt(111). *Phys. Rev. B* **56**, 12589 (1997).
- 38 Kemmer, J. *et al.* Structural analysis of the intermetallic surface compound CePt<sub>5</sub>/Pt(111). *Phys. Rev. B* **90**, 195401 (2014).
- 39 Przychodnia, M. *et al.* Controlled growth of Gd-Pt surface alloys on Pt(111). *Phys. Rev. B* **105**, 035416 (2022).
- 40 Tian, Q. *et al.* Twist-Angle Tuning of Electronic Structure in Two-Dimensional Dirac Nodal Line Semimetal Au<sub>2</sub>Ge on Au(111). *ACS Nano* **18**, 9011-9018 (2024).
- 41 Xie, Y. *et al.* Spectroscopic signatures of many-body correlations in magic-angle twisted bilayer graphene. *Nature* **572**, 101-105 (2019).
- 42 Wang, Y., Wu, H., McCandless, G. T., Chan, J. Y. & Ali, M. N. Quantum states and intertwining phases in kagome materials. *Nat. Rev. Phys* **5**, 635-658 (2023).
- 43 Wu, Q., Zhang, S., Song, H.-F., Troyer, M. & Soluyanov, A. A. WannierTools: An open-source software package for novel topological materials. *Comput. Phys. Commun.* **224**, 405-416 (2018).
- 44 Zhao, C. *et al.* Coexistence of Robust Edge States and Superconductivity in Few-Layer Stanene. *Phys. Rev. Lett.* **128**, 206802 (2022).
- 45 Kresse, G. & Furthmüller, J. Efficiency of *ab-initio* Total Energy Calculations for Metals and Semiconductors Using a Plane-Wave Basis Set. *Comput. Mater. Sci.* **6**, 15-50 (1996).
- 46 Perdew, J. P., Burke, K. & Ernzerhof, M. Generalized Gradient Approximation Made Simple. *Phys. Rev. Lett.* **77**, 3865 (1996).
- 47 Grimme, S., Antony, J., Ehrlich, S. & Krieg, H. A Consistent and Accurate *ab initio* Parametrization of Density Functional Dispersion Correction (DFT-D) for the 94 Elements H-Pu. *J. Chem. Phys.* **132**, 154104 (2010).